Supporting Information

Quantitative Imaging of Lipid Synthesis and Lipolysis Dynamics in *Caenorhabditis elegans* by Stimulated Raman Scattering Microscopy

Xuesong Li,[†,‡,⊥] Yan Li,[§,⊥] Meijuan Jiang,[∥,⊥] Wanjie Wu,[†,‡] Sicong He,[†,‡] Congping Chen,[†,‡] Zhongya Qin,[†,‡] Ben Zhong Tang,[∥] Ho Yi Mak,[*,§] and Jianan Y. Qu[*,†,‡]

[†]*Department of Electronic and Computer Engineering, Hong Kong University of Science and Technology, Clear Water Bay, Kowloon, Hong Kong 999077, China*

[‡]*Center of Systems Biology and Human Health, School of Science and Institute for Advanced Study, Hong Kong University of Science and Technology, Clear Water Bay, Kowloon, Hong Kong 999077, China*

[§]*Division of Life Science, Hong Kong University of Science and Technology, Clear Water Bay, Kowloon, Hong Kong 999077, China*

[∥]*Department of Chemistry, Hong Kong University of Science and Technology, Clear Water Bay, Kowloon, Hong Kong 999077, China*

[⊥]*The authors contributed equally.*

[*]*Correspondence email: hym@ust.hk (Mak, H.Y.) and eequ@ust.hk (Qu, J.Y.)*

Materials and Methods

Setup of the hsSRS Microscope System. Our hsSRS microscope system, as shown in Figure 1A, was set up as follows: A mode-locked Ytterbium fiber laser, centered at 1031 nm with a 5.2-picosecond (ps) pulse duration and 80-MHz repetition rate, was coupled into an integrated optical parametric oscillator (OPO, *pico*Emerald S; APE, Berlin, Germany). The Yb-fiber laser was first compressed to the Fourier limit with a 2-ps pulse duration and 10-cm^{-1} bandwidth, and then frequency doubled to pump the OPO in a ring cavity layout. The OPO signal output was tunable from 780 nm to 960 nm, and termed as the pump beam in SRS. Meanwhile, a portion of the 1031-nm fundamental laser was modulated by a built-in electro-optical modulator (EOM) at 20 MHz and served as the Stokes beam. The pump and Stokes beams were combined with a dichroic mirror inside the OPO and maintained spatiotemporal overlapping. After collimation, magnification and power regulation, two beams were directed into a home-made laser scanning microscope. A pair of 3-mm galvanometer scanners (6215H, Cambridge Technology) and optical relay system (scan lens: SL50-2P2; tube lens: TTL200-B-SP, Thorlabs) achieved the raster scanning of samples. A high-N.A. 40× water immersion objective (UAPO40XW3/340, 1.15 N.A., Olympus) with high near-IR transmission was used throughout this study. The forward-going pump and Stokes beams after passing through the sample were collected in transmission with a high N.A. oil immersion condenser (UAAC, Achromat/aplanat condenser, 1.4 N.A., Olympus) following Köhler illumination. Two filters (86108 shortpass at 975-nm OD4, Edmund Optics; FF01-850/310, SRS imaging emission filter, Semrock) blocked the Stokes beam and purified the pump beam in front of the large area Si-photodiode (10 mm^2, APE, Berlin, Germany). A fast analog lock-in amplifier (LIA) demodulated the SRS signals in phase with the EOM. An acquisition card (PCIe-6363, National Instruments, Austin, TX) collected the amplitude output from the LIA at each pixel to reconstruct a single image. One frame consisted of 512 × 512 pixels with a 25.6-μs pixel dwelling time under a 20-μs time constant of the LIA.

Since the 2-ps laser pulses could also excite two-photon-excited fluorescence (TPEF), we added a fluorescence lifetime imaging (FLIM) module to record the autofluorescence signals in *C. elegans*. A dichroic mirror (FF665-Di02, Semrock) was placed above the objective to reflect the TPEF signals to a hybrid photomultiplier tube (PMT) detector and a time-correlated single photon counting (TCSPC) module (HPM-100-40 and SPC-150, Becker & Hickl GmbH) for photon counts recording. The LROs-dominated TPEF signals were selected by a short-pass filter (FF01-680/SP, Semrock) and a band-pass filter (FF03-525/50, Semrock). The detection principles of FLIM and SRS are shown upper and lower frames in Figure 1B, respectively.

Hyperspectral Imaging. Wavelength-sweeping was used for hyperspectral mode to characterize the SRS properties of different fatty acids. By tuning the OPO crystal temperature, cavity length and Lyot filter steps, the wavelength of the pump beam was tuned at the accuracy as fine as 0.2 nm per step. It usually took 5 to 10 seconds to complete one wavelength step. The laser power was monitored and remained constant during the entire sweeping process. The final hsSRS spectrum was reconstructed based on the averaged results over five repeated sweeps.

Two-wavelength SRS Subtraction. Apparently, the normal wavelength-sweeping mode is too slow for subcellular imaging of live *C. elegans*. Inspired by previous works,[1-2] we therefore developed a fast OPO tuning technique which can rapidly obtain two SRS images under two different Raman shifts. By only adjusting the Lyot filter, the wavelength of the pump beam could be tuned up to 4.6 nm, corresponding to 65 cm^{-1} in less than three seconds. This tuning range defined the maximal separation in wavenumber between the "on-resonant" Raman peak of a bioorthogonal fatty acid and "off-resonant" non-Raman background. The on-resonant and off-resonant SRS images were automatically acquired through synchronizing the Lyot filter to the frame trigger, which was precisely controlled by a self-written C# program. As shown in Figure 1C, a pair of "on-resonant" and "off-resonant" images could be acquired with a short switching time (< 3 s) to avoid motion artifacts of the worms. The genuine C-D or C≡C SRS signals (I_{SRS}) were generated by subtracting the off-resonant signals (I_{OFF}) from the on-resonant signals (I_{ON}).
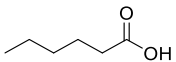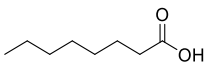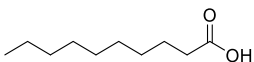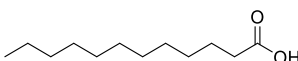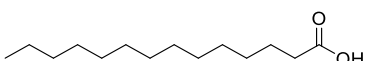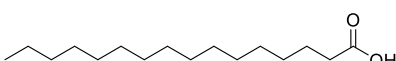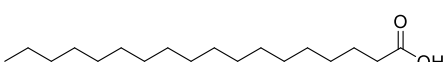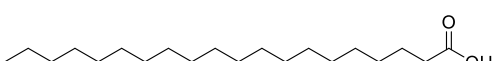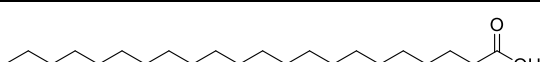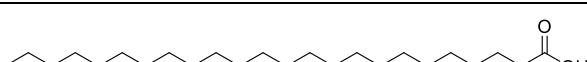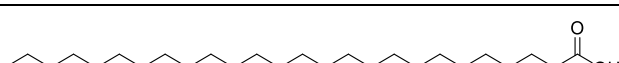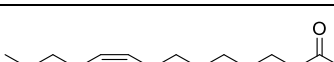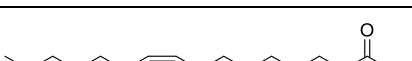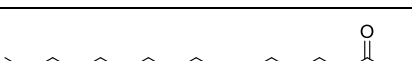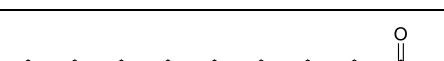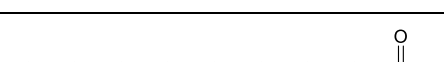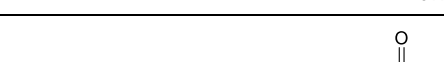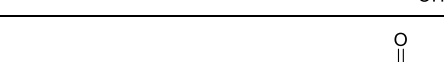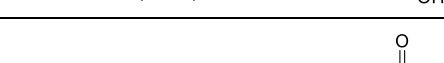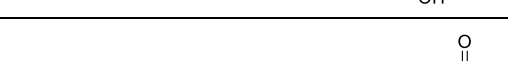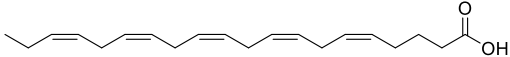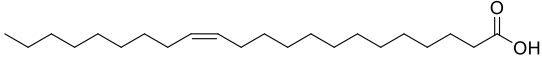
Supplementary Figures and Tables
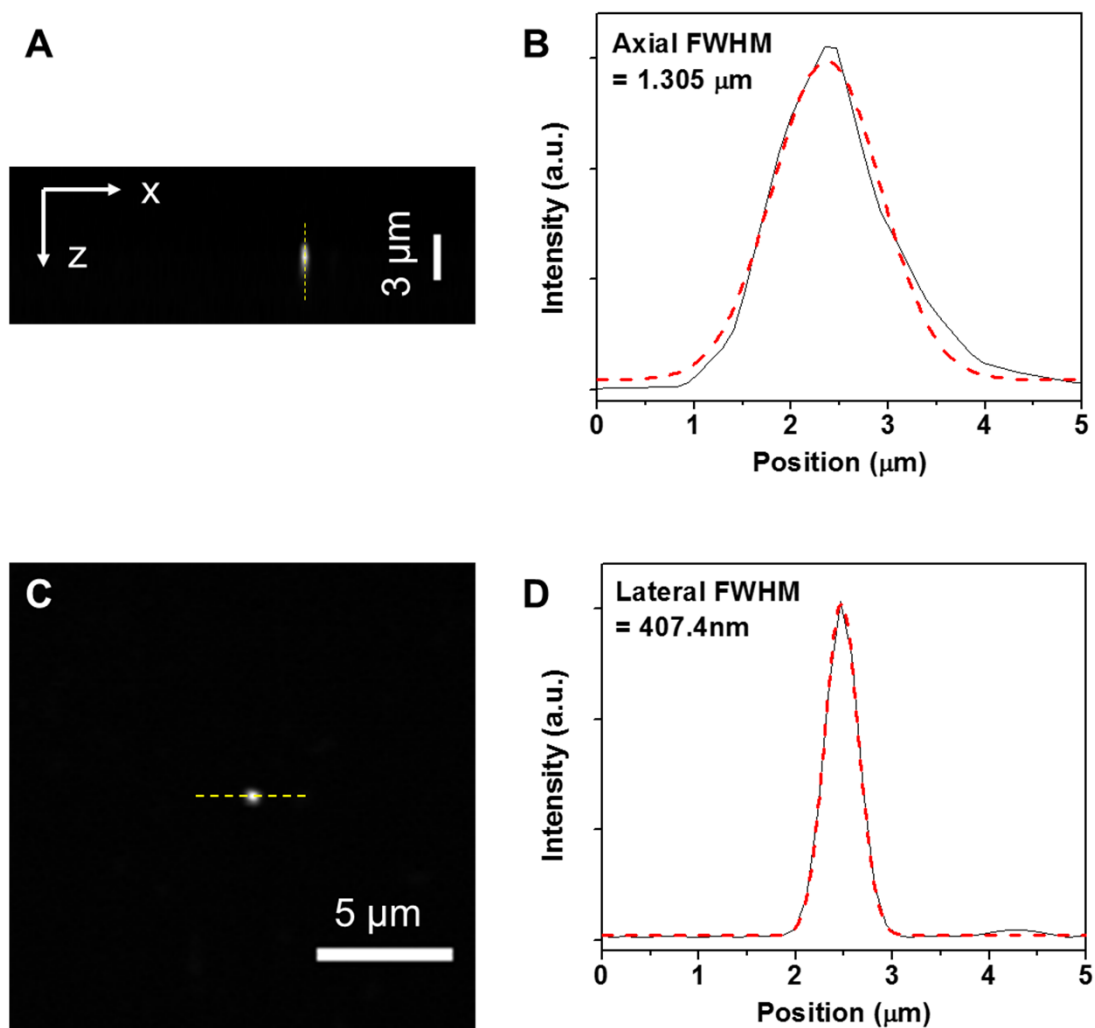
Figure S1. Spatial resolution of the SRS microscope. (A) Depth-resolved SRL imaging of 200 nm polystyrene beads. (B) Gaussian fit of the intensity profile along the z axis indicated by the dash line in (A). (C) SRS image in XY plane of the same sample. (D) Gaussian fit of the dash line in (C) of a 200 nm bead.

**Table S1.** Raman peak areas of different deuterated fatty acids [a]

Fatty acids	Chemical structures	C-D number of all-deuterated fatty acids	Raman peak areas
Acetic acid		3	30.63857
Butanoic acid		7	74.13874

Hexanoic acid		11	115.2551
Caprylic acid		15	151.4214
Capric acid		19	186.7691
Lauric acid		23	221.7151
Myristic acid		27	256.4468
Palmitic acid		31	291.036
Stearic acid		35	325.5118
Arachidic acid		39	359.896
Behenic acid		43	394.2536
Lignoceric acid		47	428.5431
Cerotic acid		51	462.8669
Myristoleic acid		25	240.7146
Palmitoleic acid		29	283.486
Sapienic acid		29	275.1177
Oleic acid		33	309.4746
Elaidic acid		33	320.9318
Vaccenic acid		33	320.687
Linoleic acid		31	302.9201
Linolaidic acid		31	315.2441
α-linolenic acid		29	281.1718
Arachidonic acid		31	312.4021

| Eicosapentaenoic acid		29	286.3141
Erucic acid		41	375.0234

[a] The calculations of the Raman spectra were performed at vacuum gas phase via ground state DFT at the basis set of B3LYP/6-31g (d, p) by Gaussian 09 program. The Raman peak areas were calculated by the integration of the spectra from 2150 to 2230 cm^{-1}.
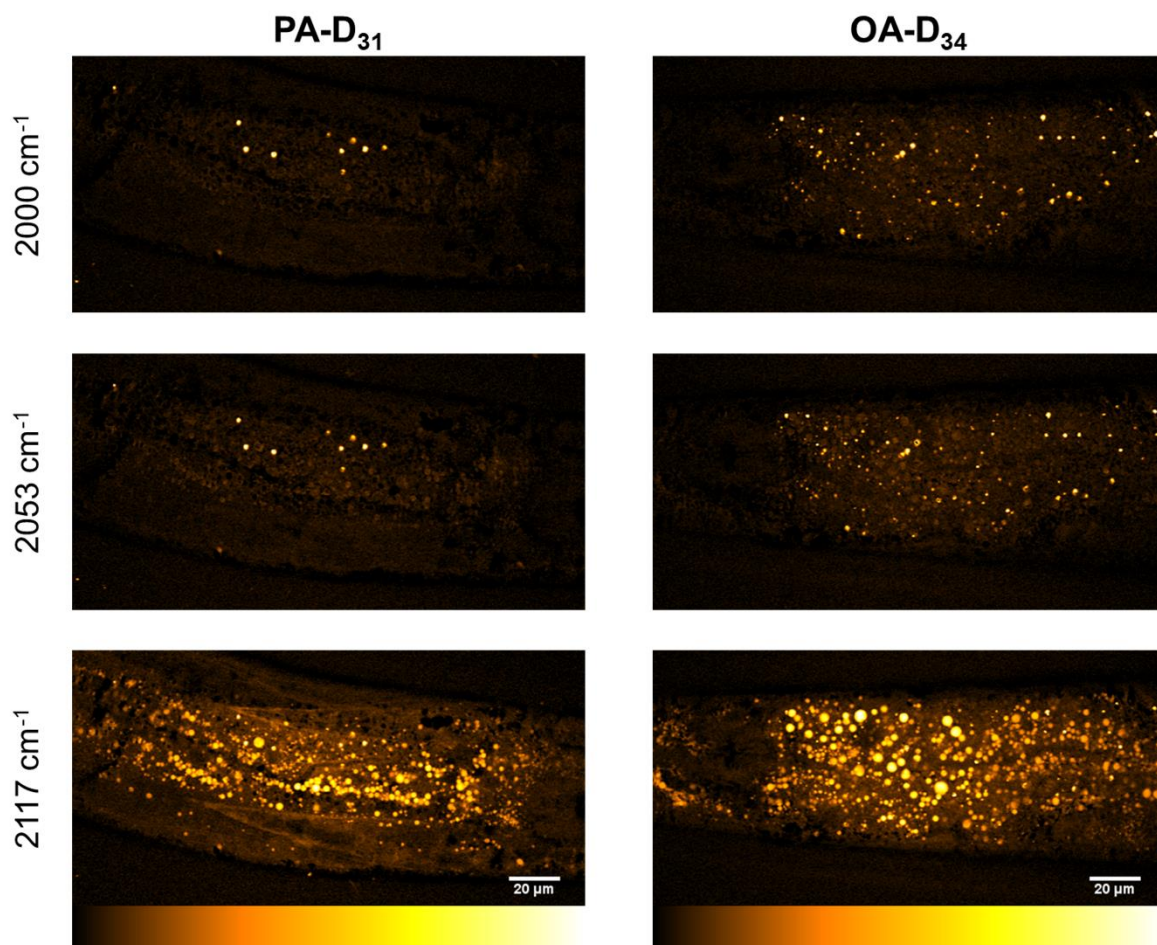

Figure S2. SRS images of wild-type *C. elegans* labeled with PA-D$_{31}$ and OA-D$_{34}$ for 25 h, in which 2000 cm^{-1} is the completely off-resonant wavenumber, 2053 cm^{-1} is the off-resonant wavenumber used in two-wavelength subtraction and 2117 cm^{-1} is the on-resonant Raman peak.
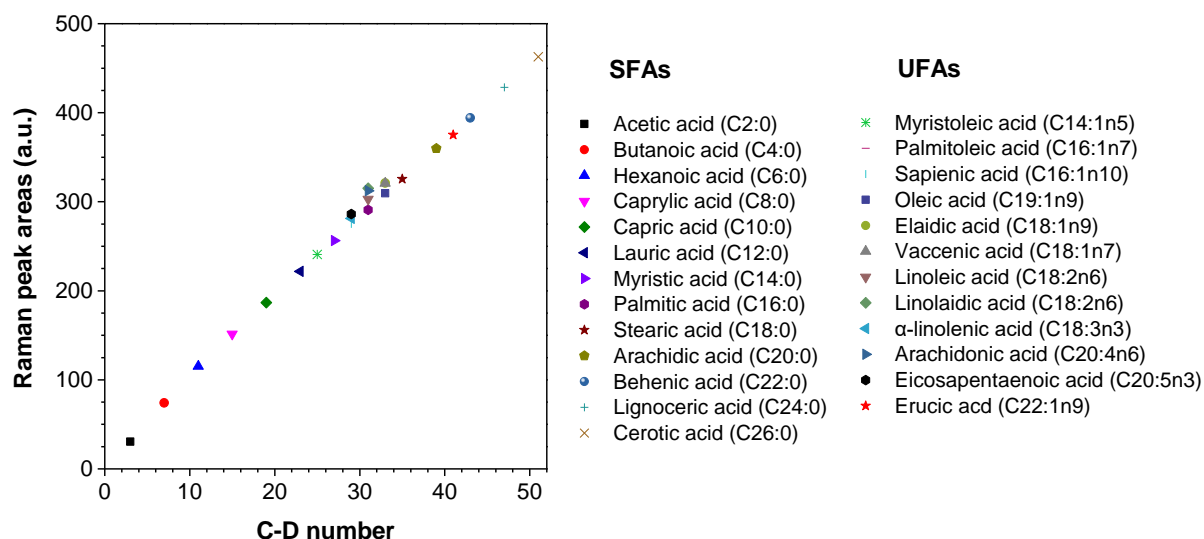
Figure S3. Plot of Raman peak areas versus C-D number of 25 different fatty acids.
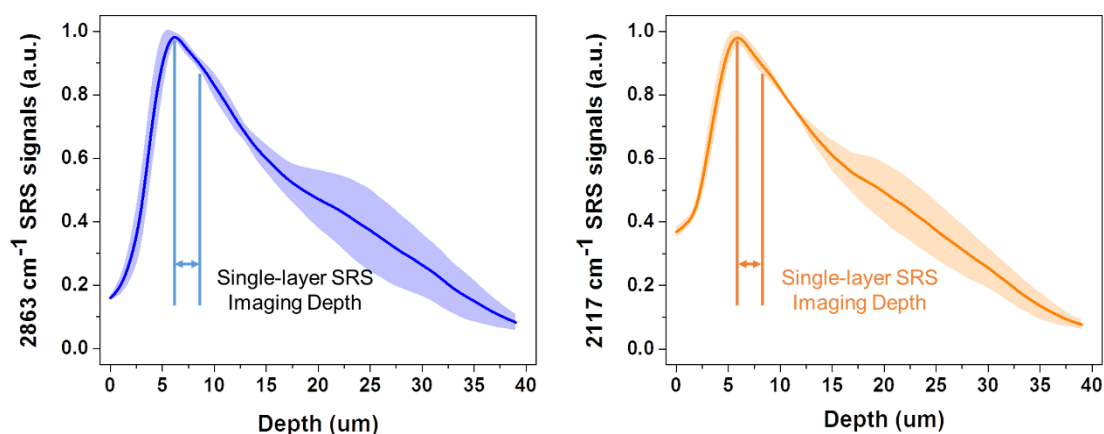
Figure S4. The average (n=3) intestinal SRS signals at different depths based on Movie S1 (2863 cm^{-1} CH$_2$ channel) and Movie S2 (2117 cm^{-1} PA-D$_{31}$ channel). The single-layer SRS imaging depth was located at 6 ~ 8 μm away from the coverslip for all animals to maintain the data consistency and to reduce the scattering and aberration effects.
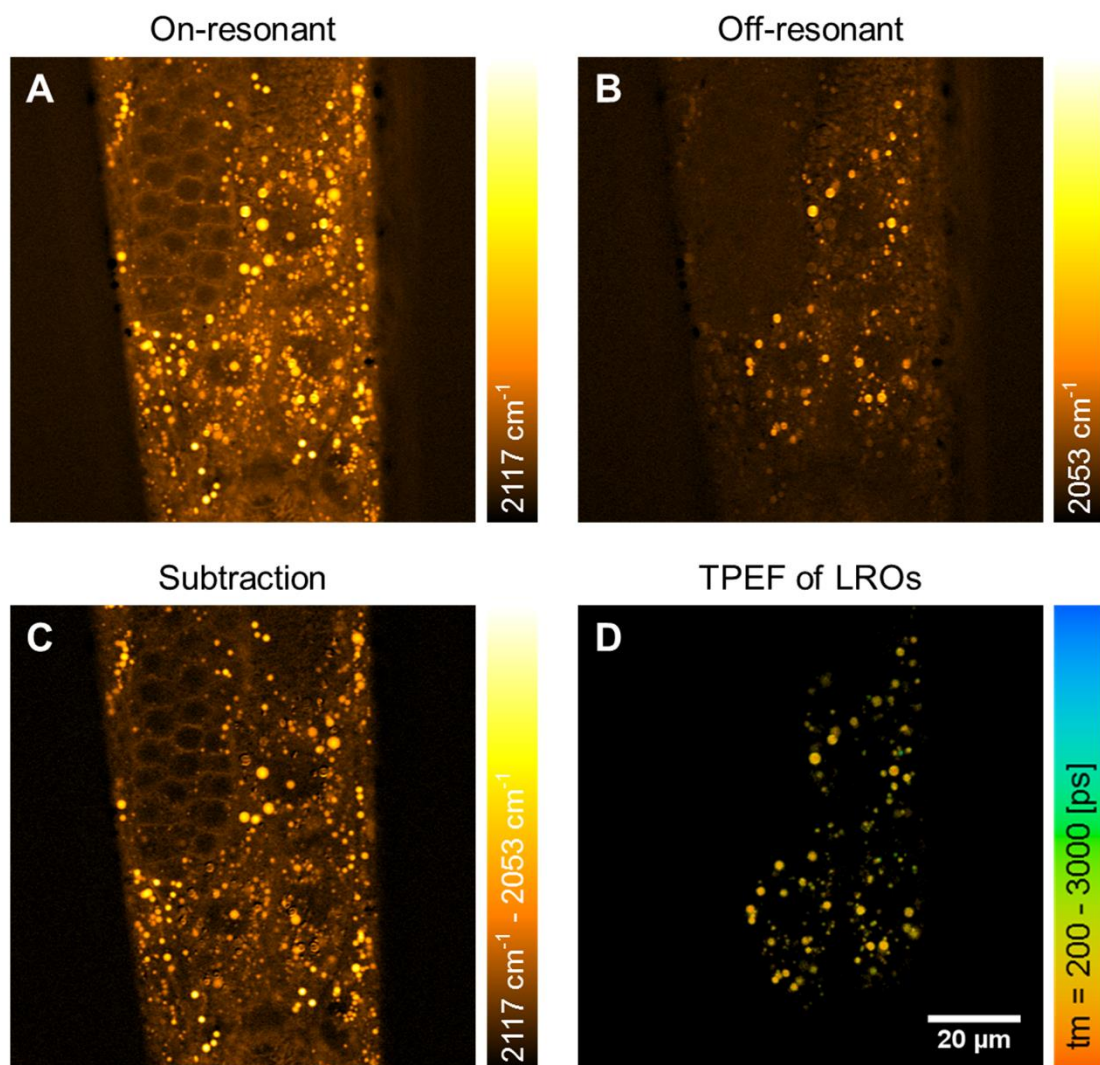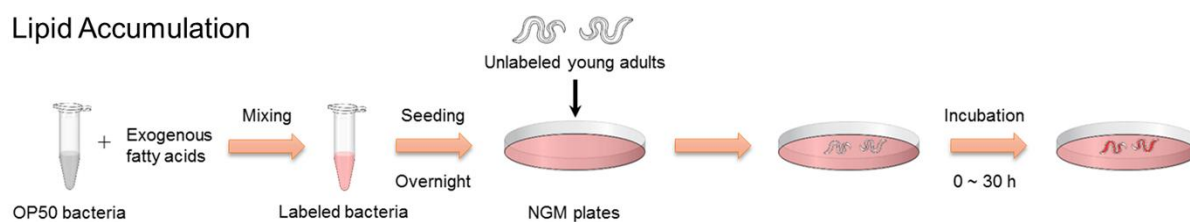
Figure S5. Representative images of *C. elegans* fed with PA-D$_{31}$ for 15 h. (A) On-resonant SRS image. (B) Off-resonant SRS image at the same site. (C) Subtraction SRS image based on (A) and (B). (D) Color-coded TPEF lifetime image of the autofluorescence from LROs.
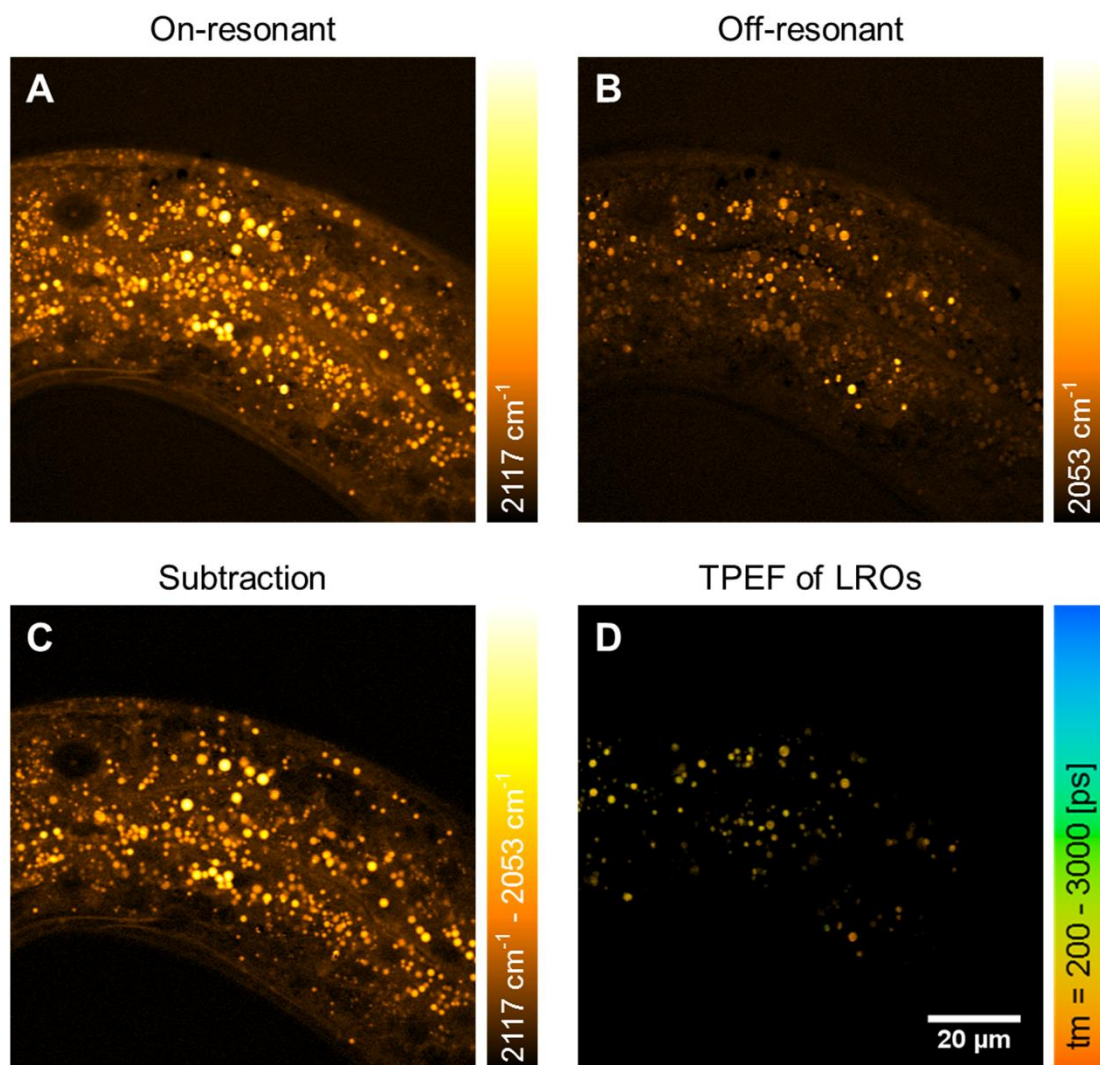
Figure S6. Representative images of *C. elegans* fed with OA-D$_{34}$ for 10 h. (A) On-resonant SRS image. (B) Off-resonant SRS image at the same site. (C) Subtraction SRS image based on (A) and (B). (D) Color-coded TPEF lifetime image of the autofluorescence from LROs.
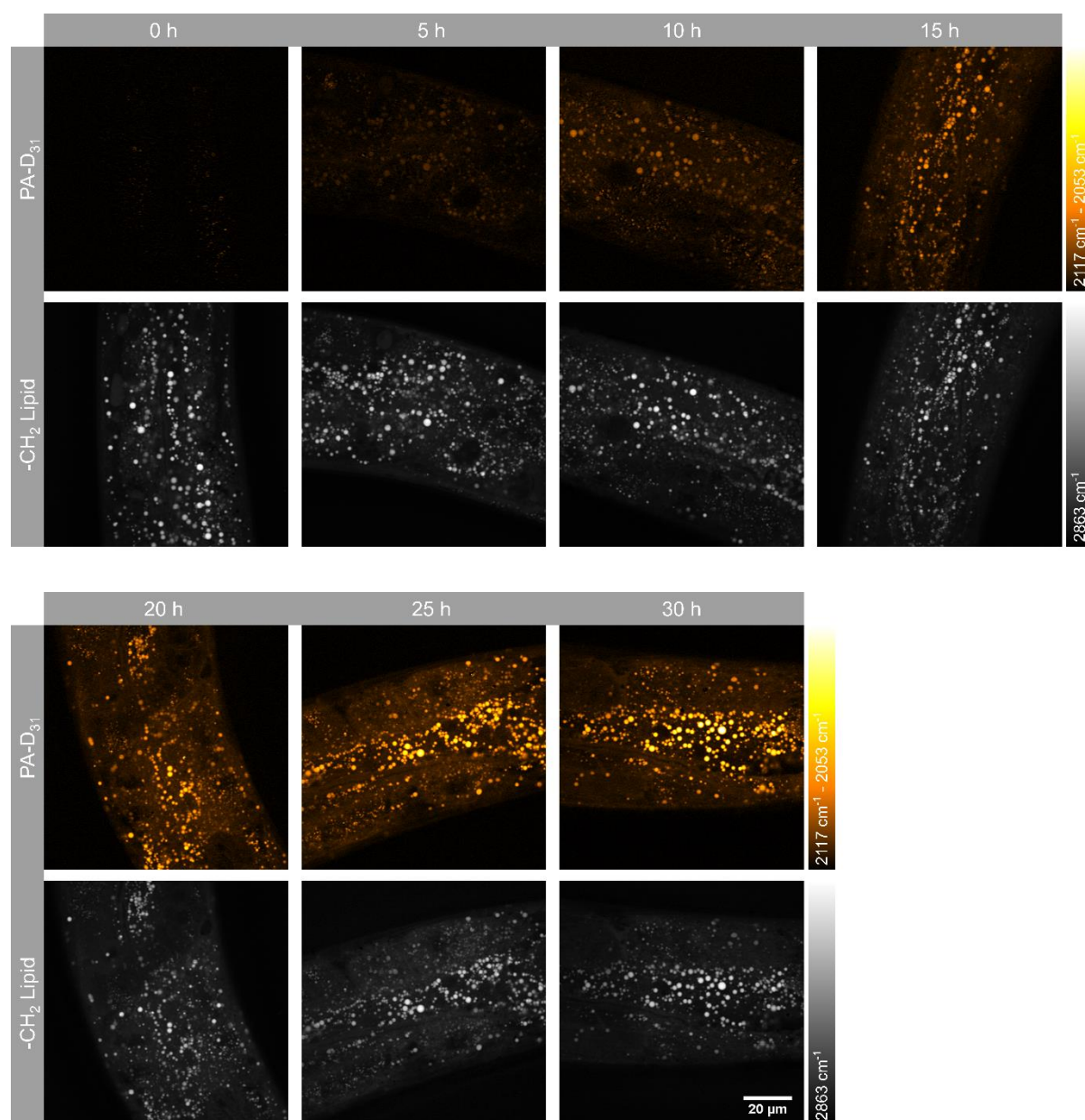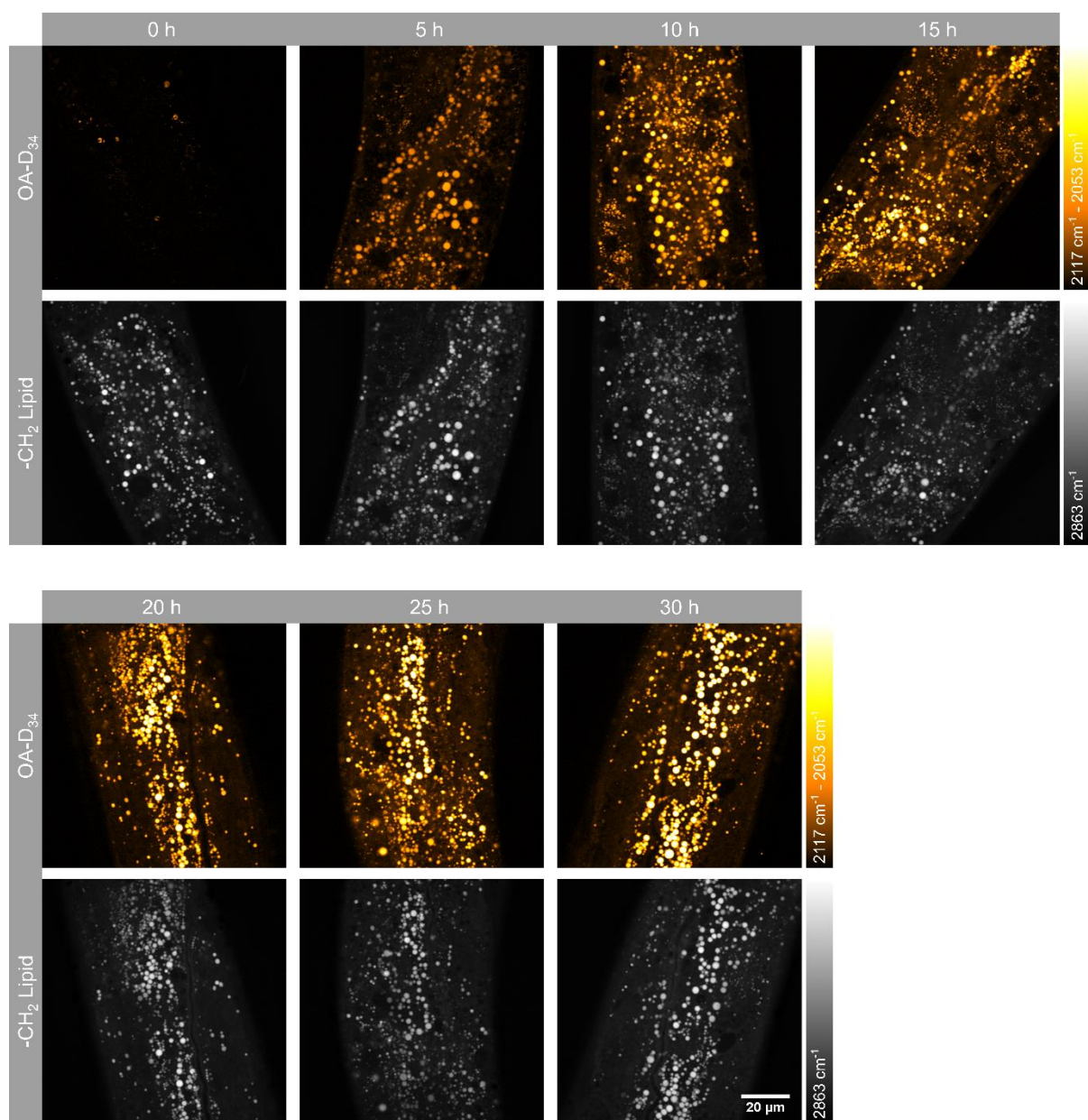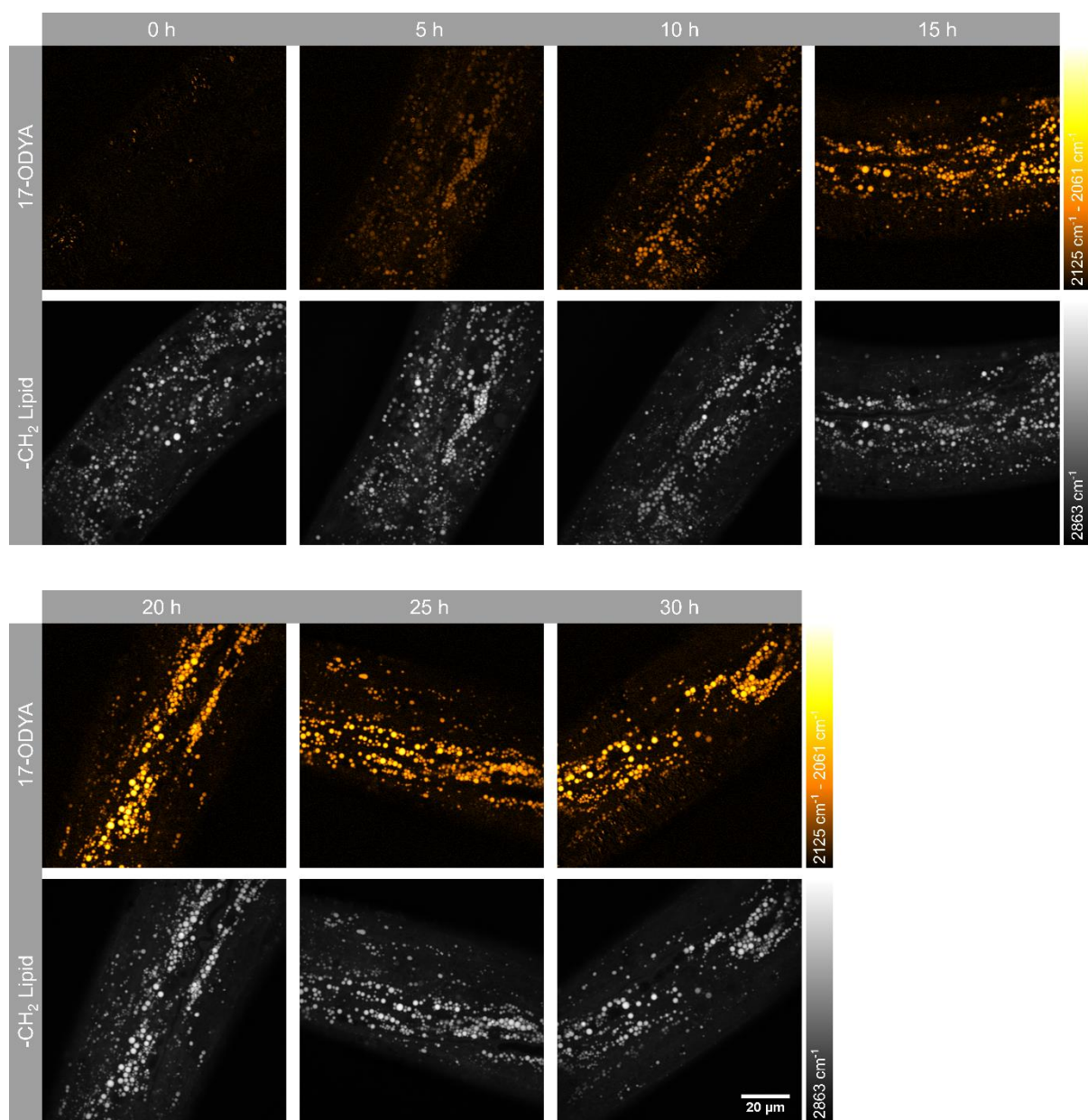
Figure S7. The experimental scheme of exogenous fatty acid supplementation in lipid accumulation experiment.
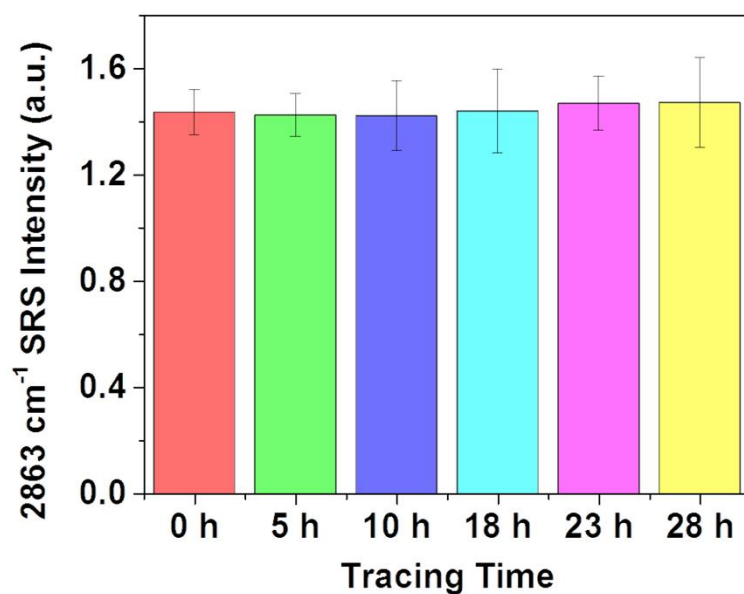

Figure S8. Representative SRS images of wild-type *C. elegans* fed with PA-D$_{31}$ over time.
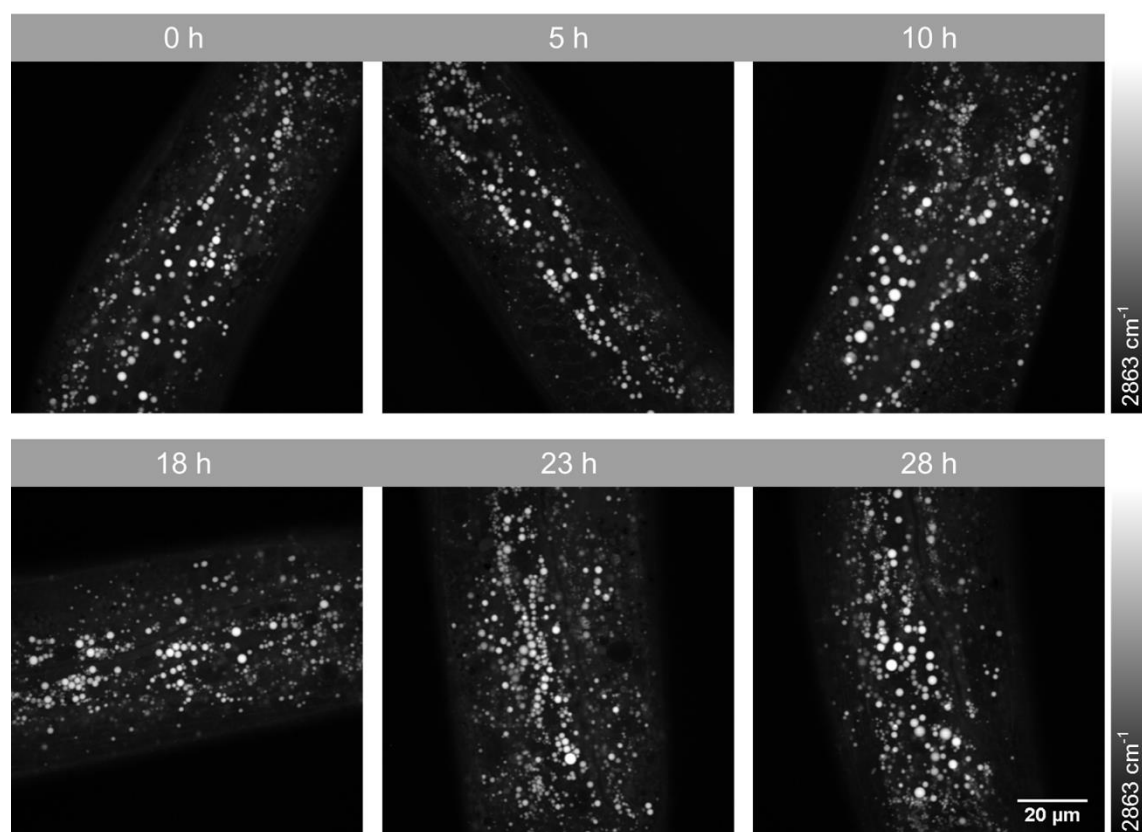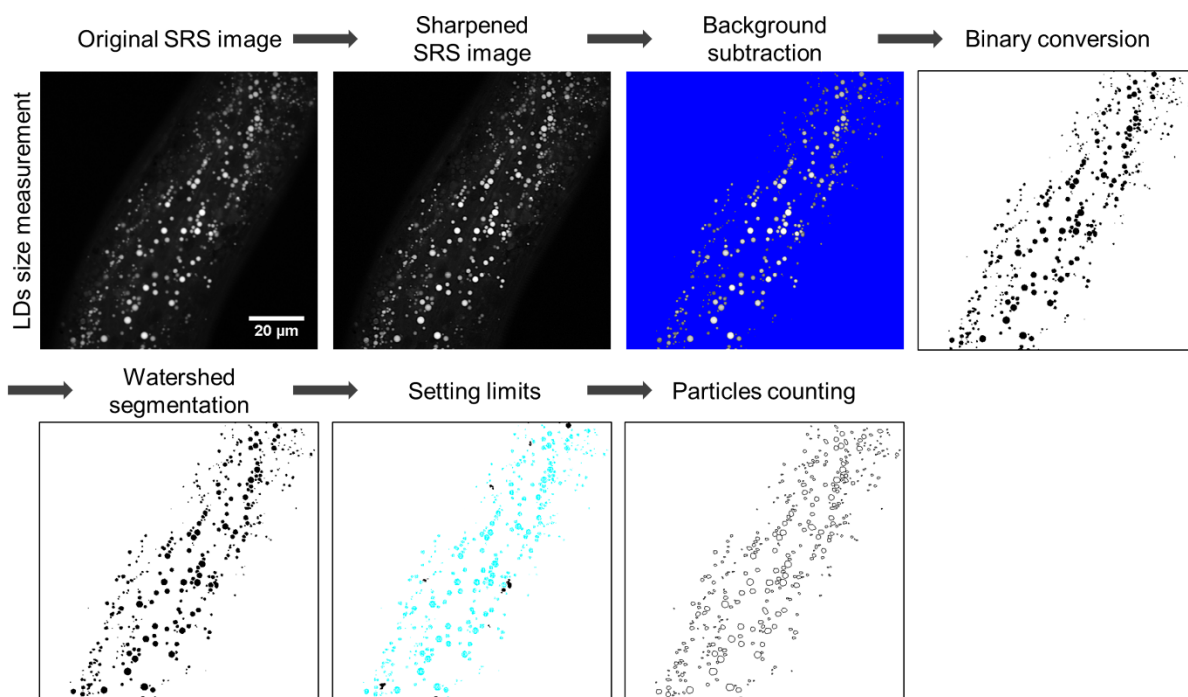
Figure S9. Representative SRS images of wild-type *C. elegans* fed with OA-D$_{34}$ over time.

**Figure S10.** Representative SRS images of wild-type *C. elegans* fed with 17-ODYA over time.

Figure S11. SRS images of wild-type *C. elegans* grown on standard OP50. The average 2863 cm^{-1} SRS signals did not show significant intensity changes over time.

Figure S12. Quantitative measurement of LDs size in SRS microscopy with the ImageJ software. First, we sharpened the original –CH$_2$ SRS image with a weighted average of the 3×3 neighborhood to make the margin of LDs clearer and then used intensity threshold to remove the background. Then we performed watershed segmentation to separate as many adjacent LDs as possible by using Watershed plugin. For particles analysis, we manually set the circularity from 0.6 to 1.0 for all LDs and excluded those LDs on image edges. So the areas of all qualified LDs were calculated respectively and summarized to give the statistical results.
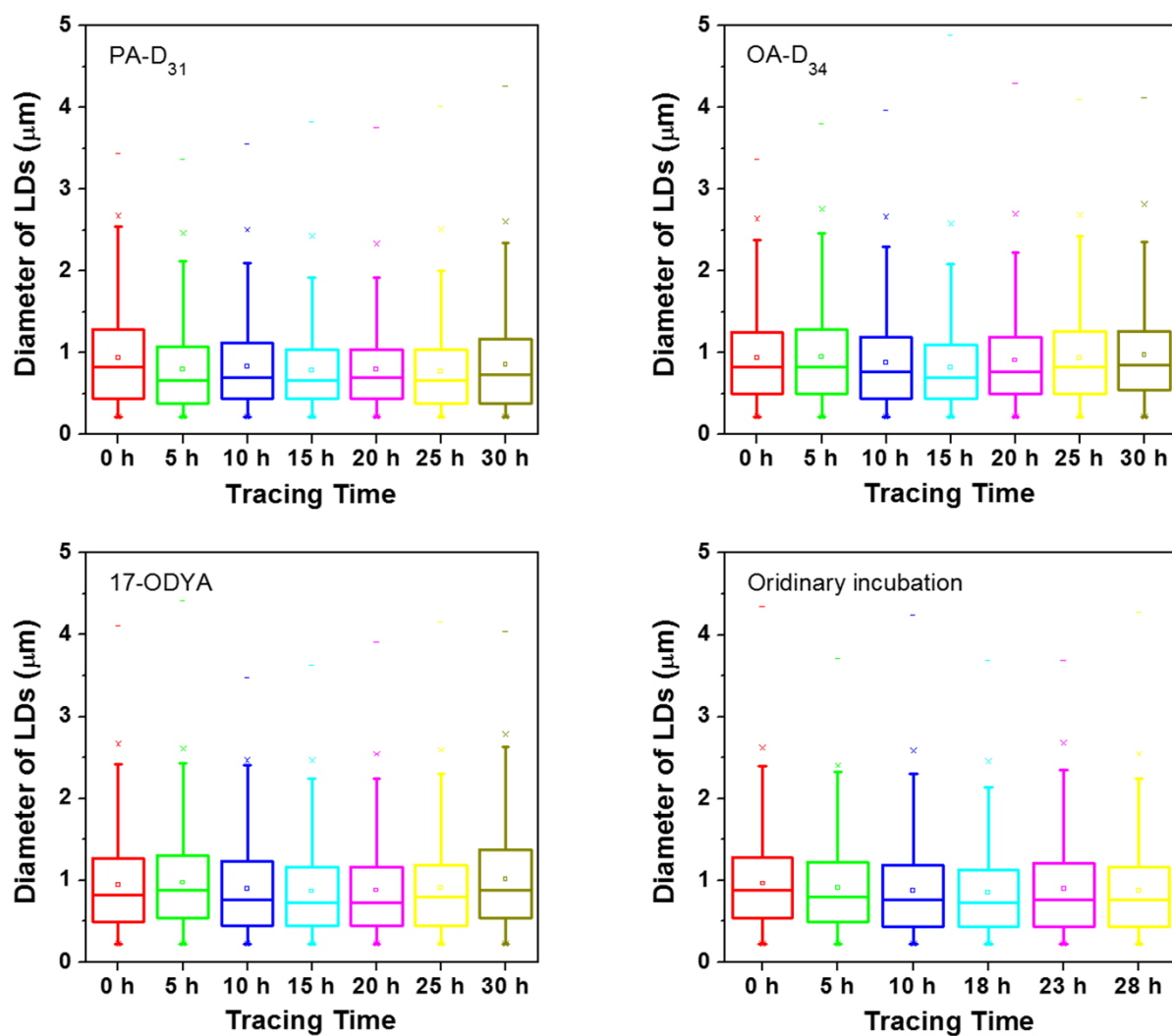
Figure S13. Quantitative analysis of the size distribution of LDs in anterior region over different incubation times. We noted that the median of diameters was always stable from 0.8 to 1 μm for all worms fed with PA-D$_{31}$, OA-D$_{34}$ or 17-ODYA. These results were consistent with the control group (worms cultured without bioorthogonal fatty acids).
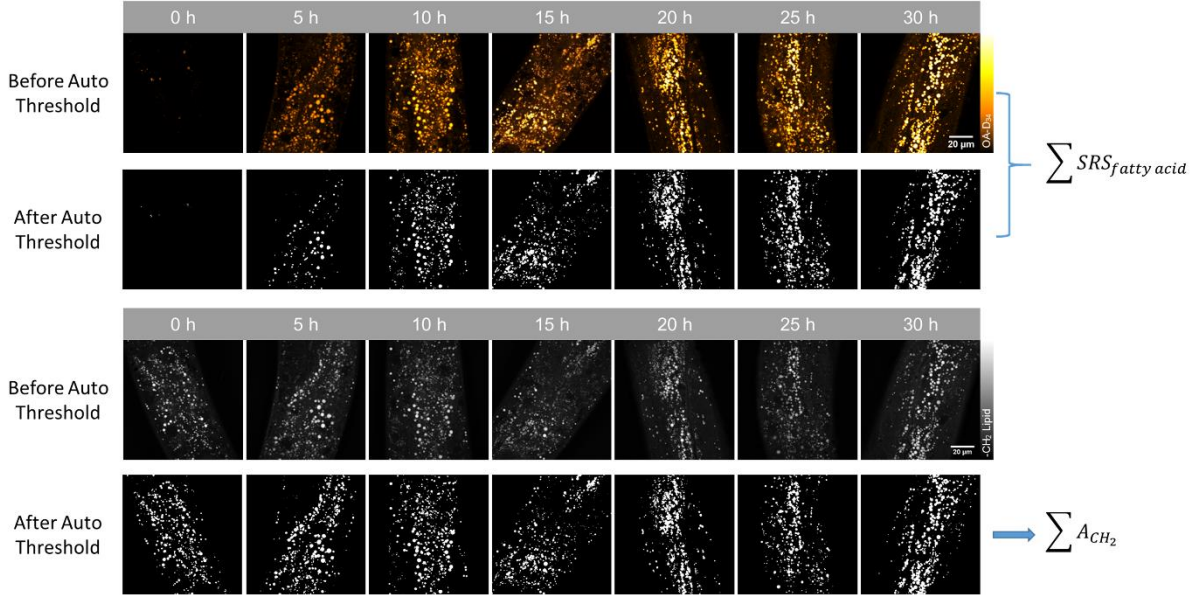
Figure S14. The average concentration of the bioorthogonal fatty acid in LDs based on image threshold. Since most of the fatty acids are stored in the form of triglycerides (TAG) in LDs, the small amounts of signals in the cytoplasm were not taken into consideration. The pixel intensity of fatty acid SRS signal in LDs of a single worm was calculated by the following equation: $I_{SRS/Pixel} = \sum SRS_{fatty\ acid} / \sum A_{CH_2}$, wherein $\sum SRS_{fatty\ acid}$ refers to the sum SRS signals of the bioorthogonal fatty acid in LDs, and $\sum A_{CH}$ refers to the area (pixels) of the total LDs determined in 2863 cm^{-1} CH$_2$ SRS channel. Therefore, $\sum A_{CH_2}$ was calculated by the sum of all LDs occupied areas in the form of pixel numbers. And $\sum SRS_{fatty\ acid}$ was directly calculated by the sum of subtracted SRS signals (PA-D$_{31}$, OA-D$_{34}$ or 17-ODYA) over the LD area. The final average concentrations of the bioorthogonal lipid molecules were derived as $\bar{c} = I_{SRS/Pixel}/slope$, in which $slope$ is identical with the calibrations in standard solutions for PA-D$_{31}$ (0.1642), OA-D$_{34}$ (0.1655) and 17-ODYA (0.0482, unit: 10^{-5} / mM), respectively. In the calculation of LD area, we applied the "Default" method of auto threshold available in ImageJ to create binary masks. The unwanted background in cytoplasm together with small LDs whose size were under the diffraction limit were not taken into consideration. And small LD-associated pixels account for only about 3% of SRS-positive pixels, so it caused negligible influence on the concentration analysis of labeled lipids. Using these image masks, we could easily calculate the total amount of bioorthogonal fatty acids in cell-silent channel and the LDs occupied areas in 2863 cm^{-1} CH$_2$ channel.
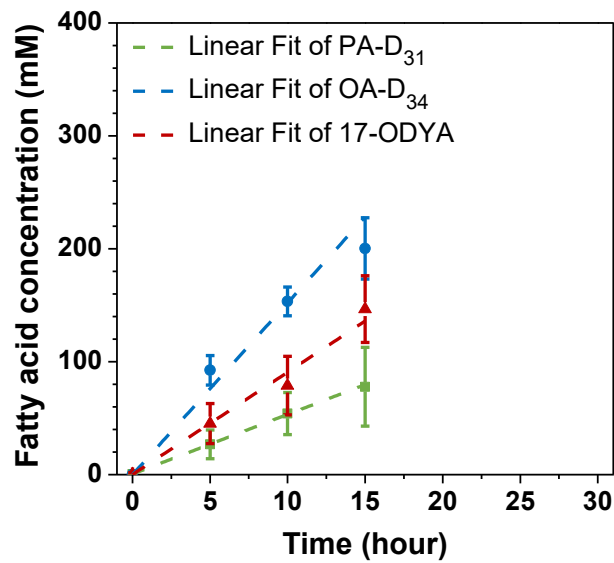
Figure S15. Linear fitting of lipid accumulation within 0 to 15 h incubation time.
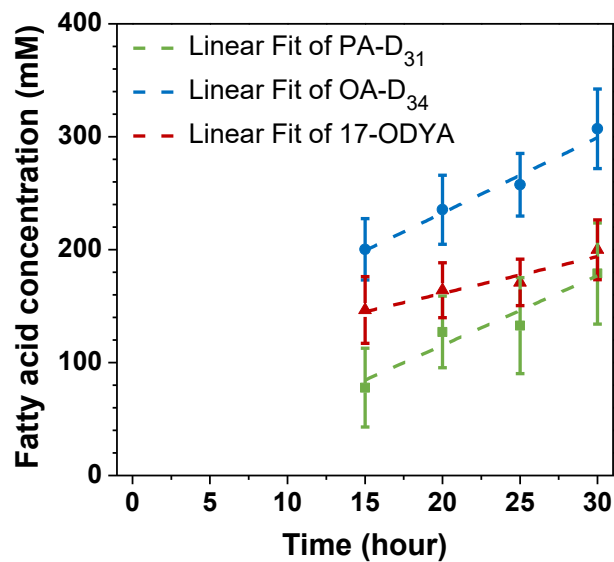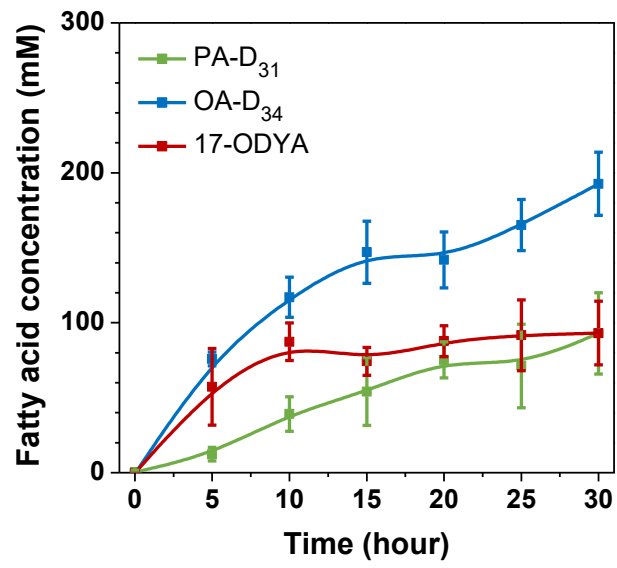

Figure S16. Linear fitting of lipid accumulation within 15 to 30 h incubation time.
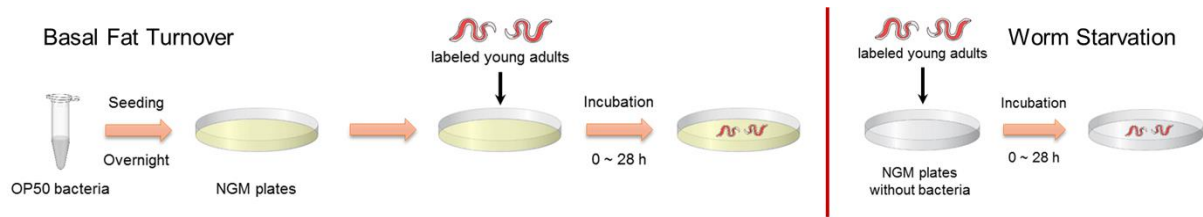
Table S2. Fatty acid accumulation rates at two different time periods.

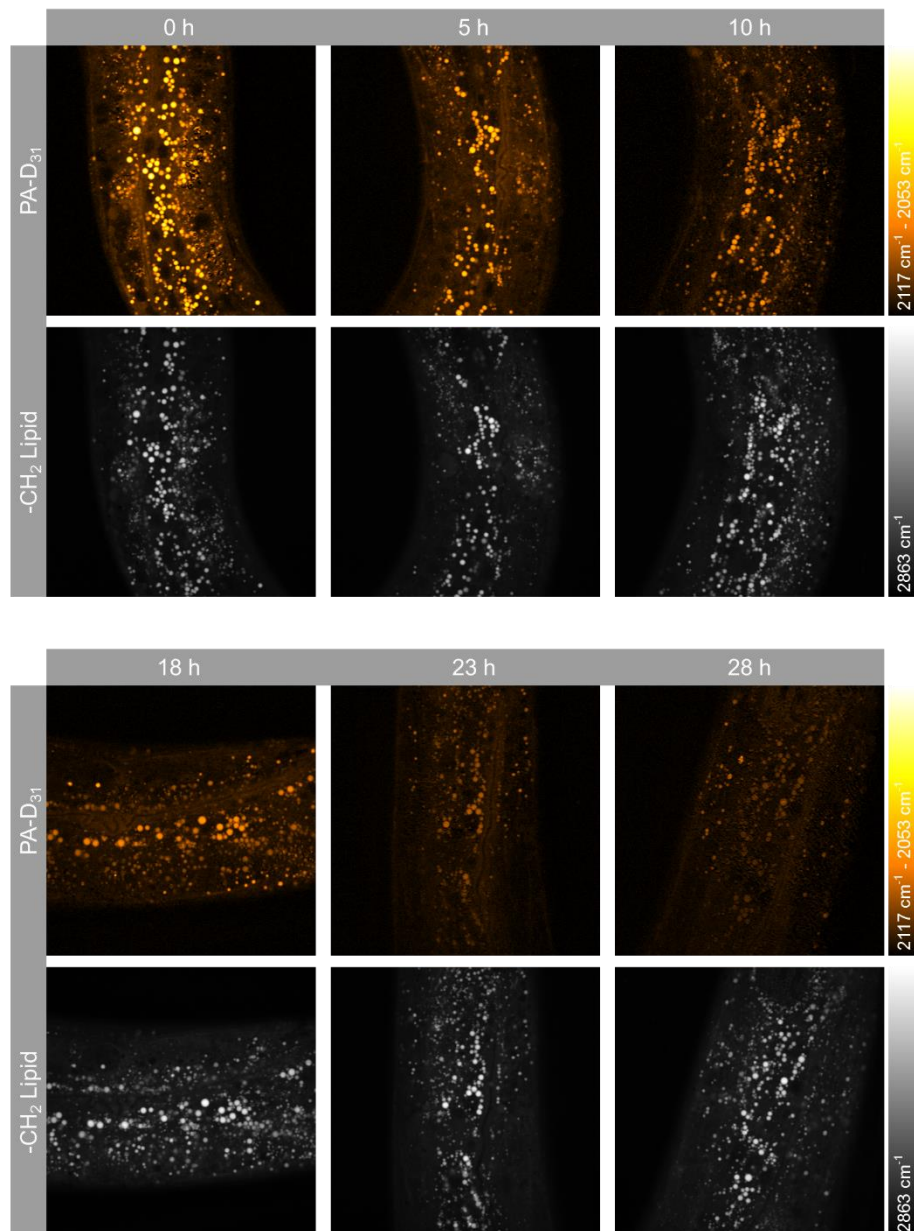| Fatty acid types	0 ~ 15 h	15 ~ 30 h
PA-D$_{31}$	5.28	6.16
OA-D$_{34}$	15.22	6.67
17-ODYA	9.07	3.26

Unit: mM / h

Figure S17. Quantitative measurement of fatty acid accumulation dynamics in the posterior region of worms (n > 12).
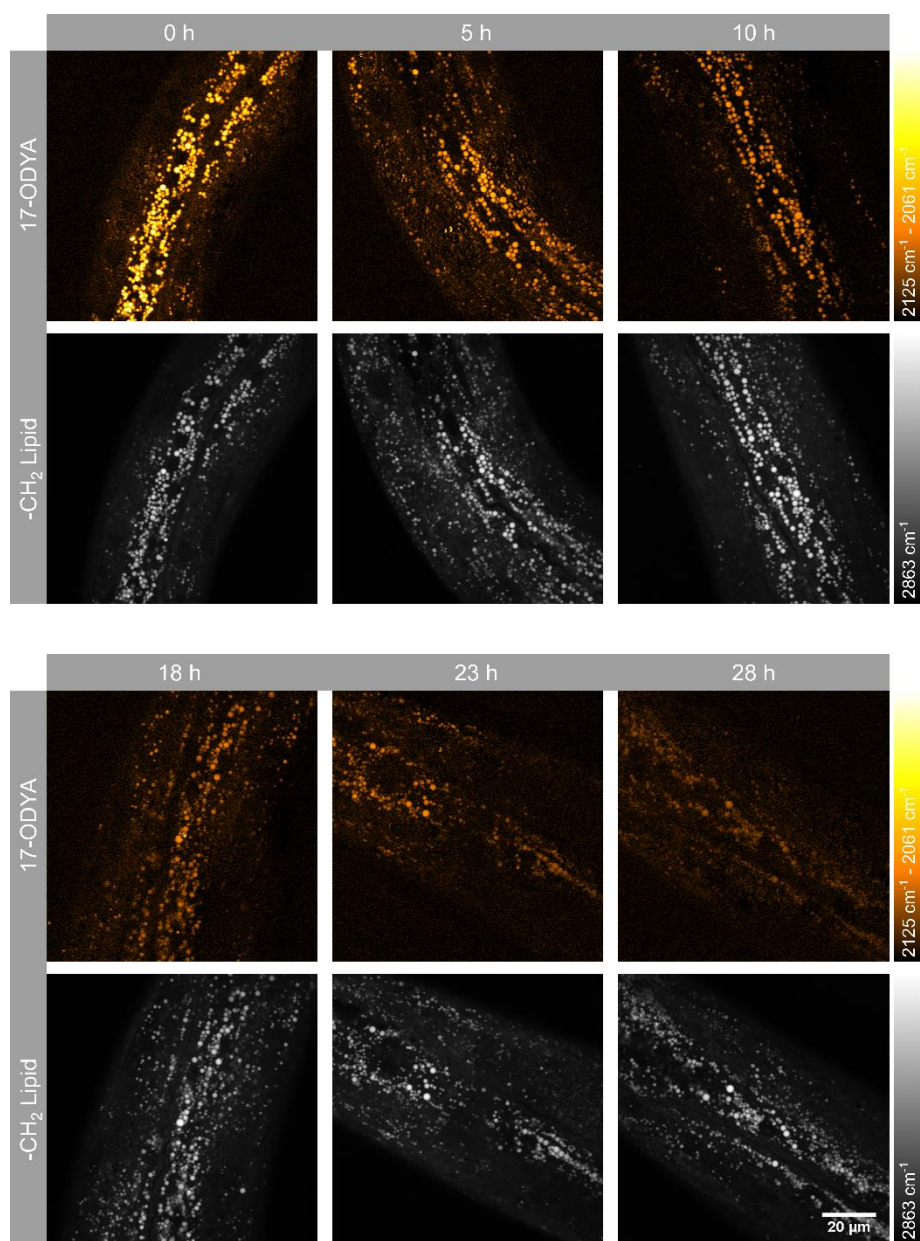
Figure S18. The experimental scheme of exogenous fatty acid supplementation in basal fat turnover and worm starvation experiments.
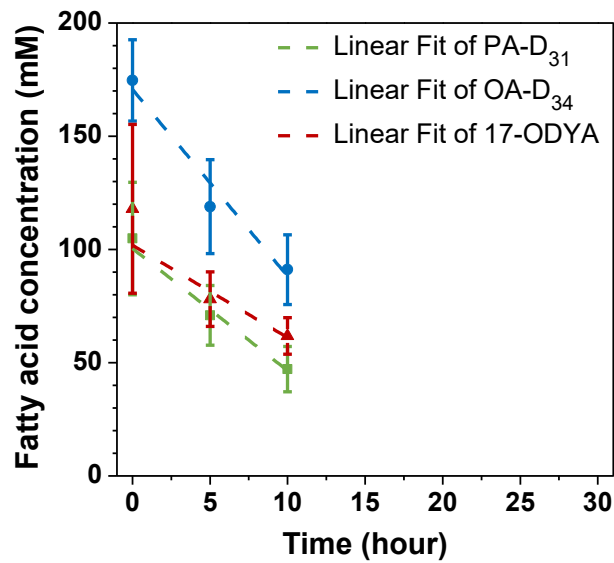

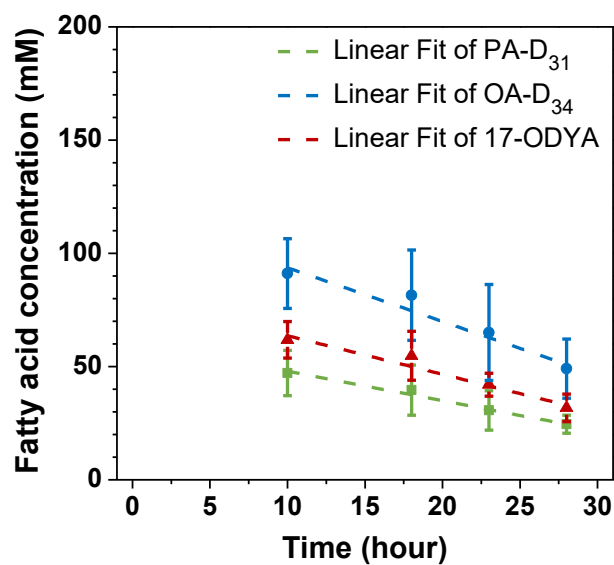**Figure S19.** Representative SRS images of PA-D$_{31}$ turnover.
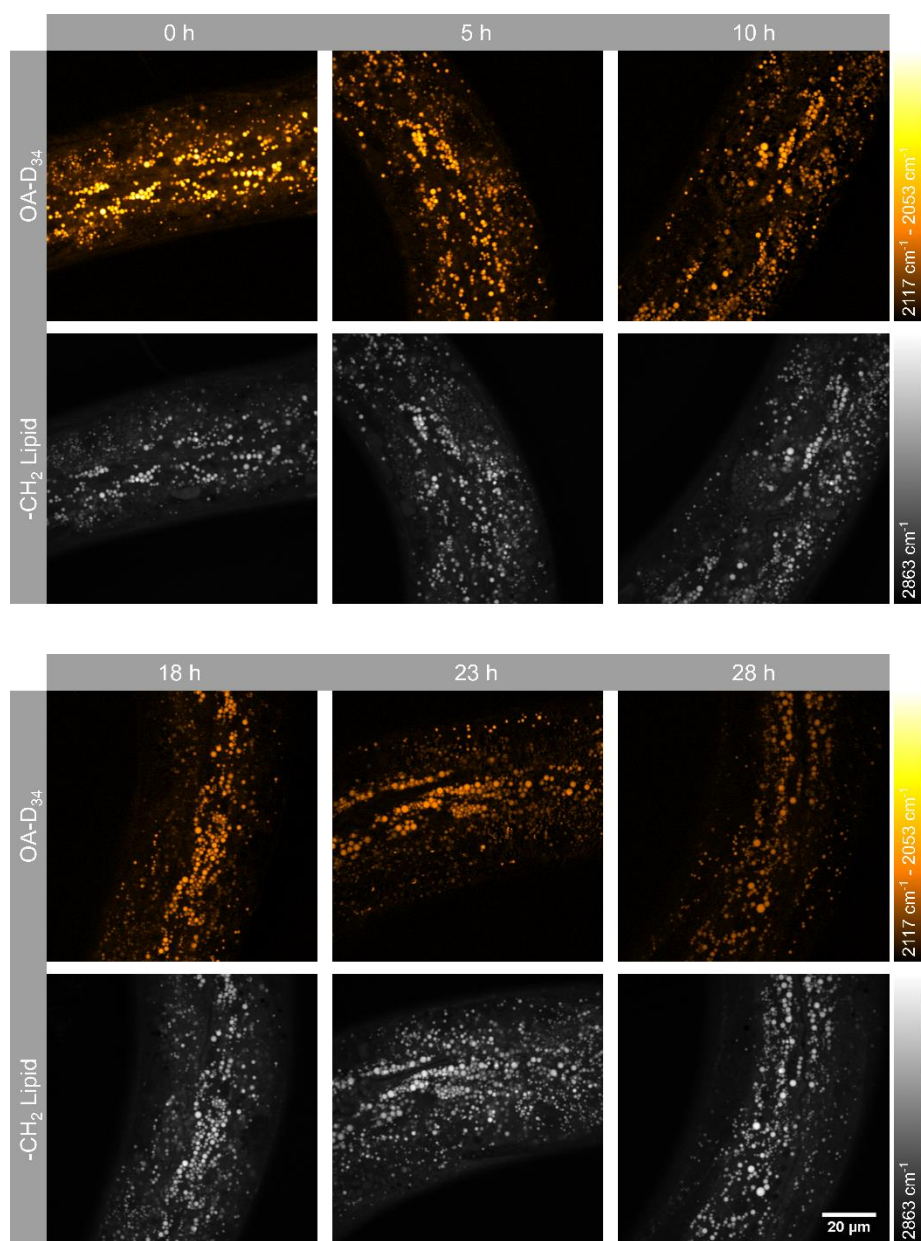
Figure S20. Representative SRS images of OA-D$_{34}$ turnover.

Figure S21. Representative SRS images of 17-ODYA turnover.

Figure S22. Linear fitting of lipid turnover within 0 to 10 h incubation time.

Figure S23. Linear fitting of lipid turnover within 10 to 28 h incubation time.

Table S3. Fatty acid turnover rates at two different time periods.

Fatty acid types	0 ~ 10 h	10 ~ 28 h
PA-D$_{31}$	5.40	1.30
OA-D$_{34}$	8.25	2.37
17-ODYA	4.08	1.70

Unit: mM / h
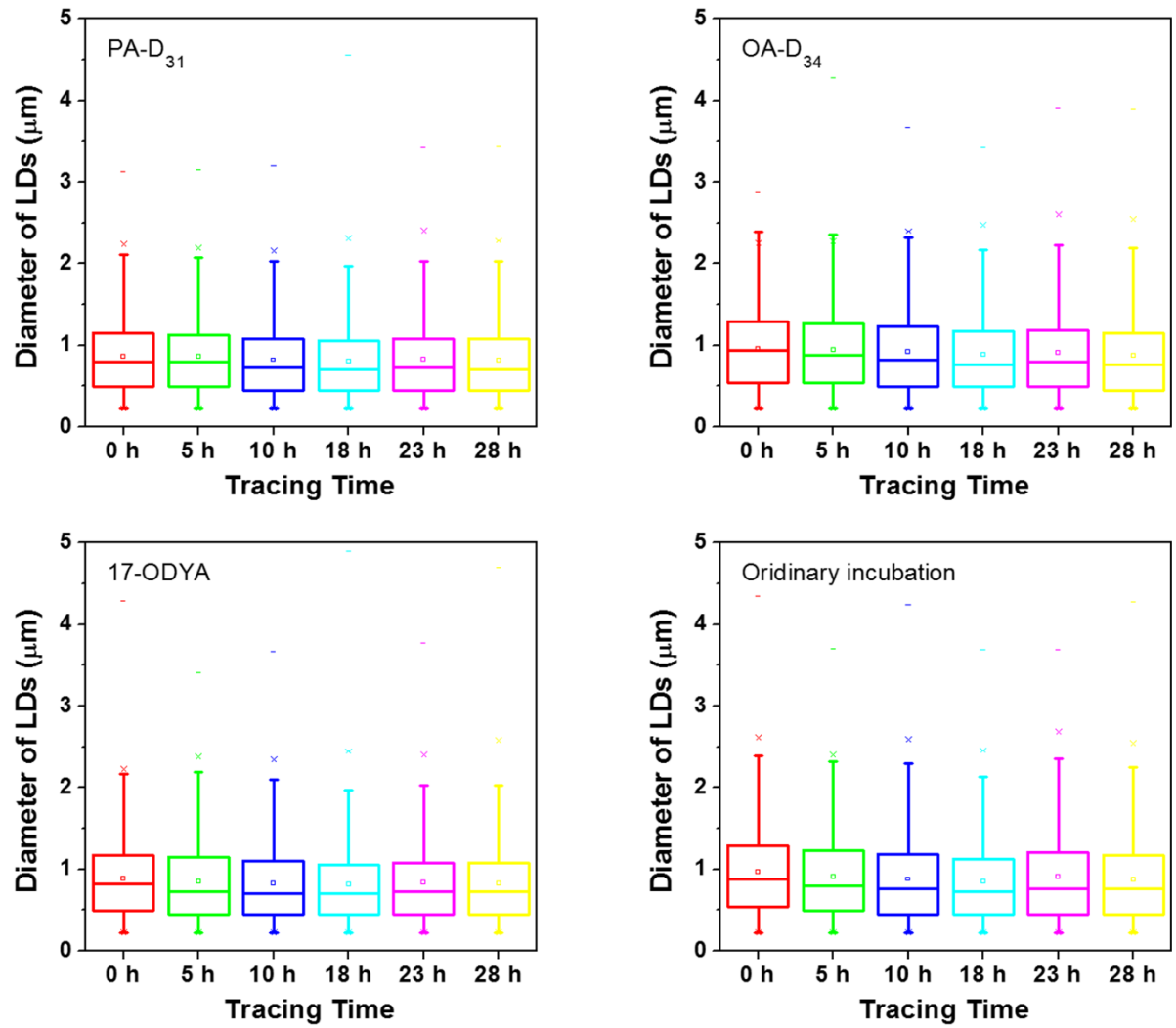
Figure S24. Quantitative analysis of the size distribution of LDs in anterior region over different incubation times.
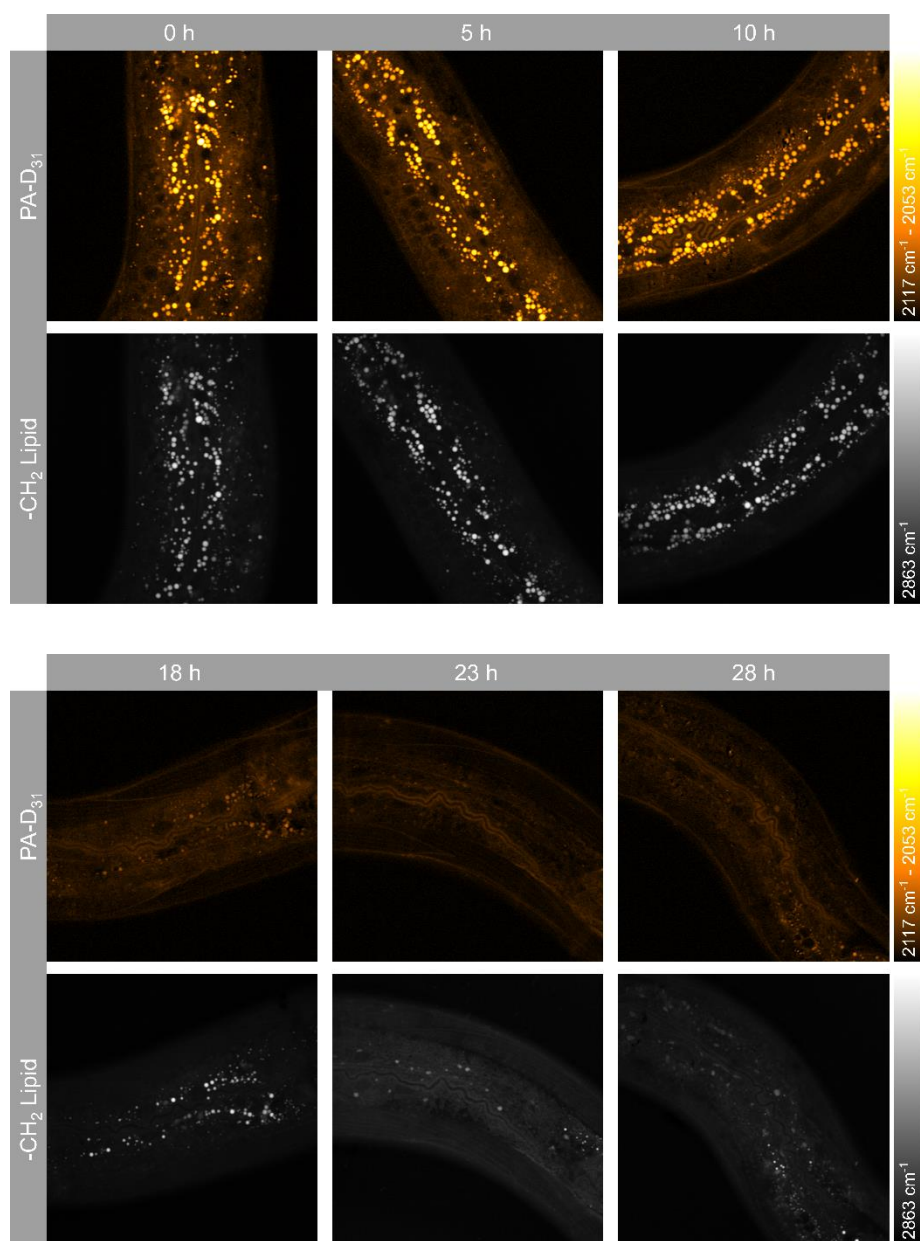
Figure S25. Representative SRS images of PA-D$_{31}$ pre-fed worms during starvation.

Figure S26. Representative SRS images of OA-D$_{34}$ pre-fed worms during starvation.

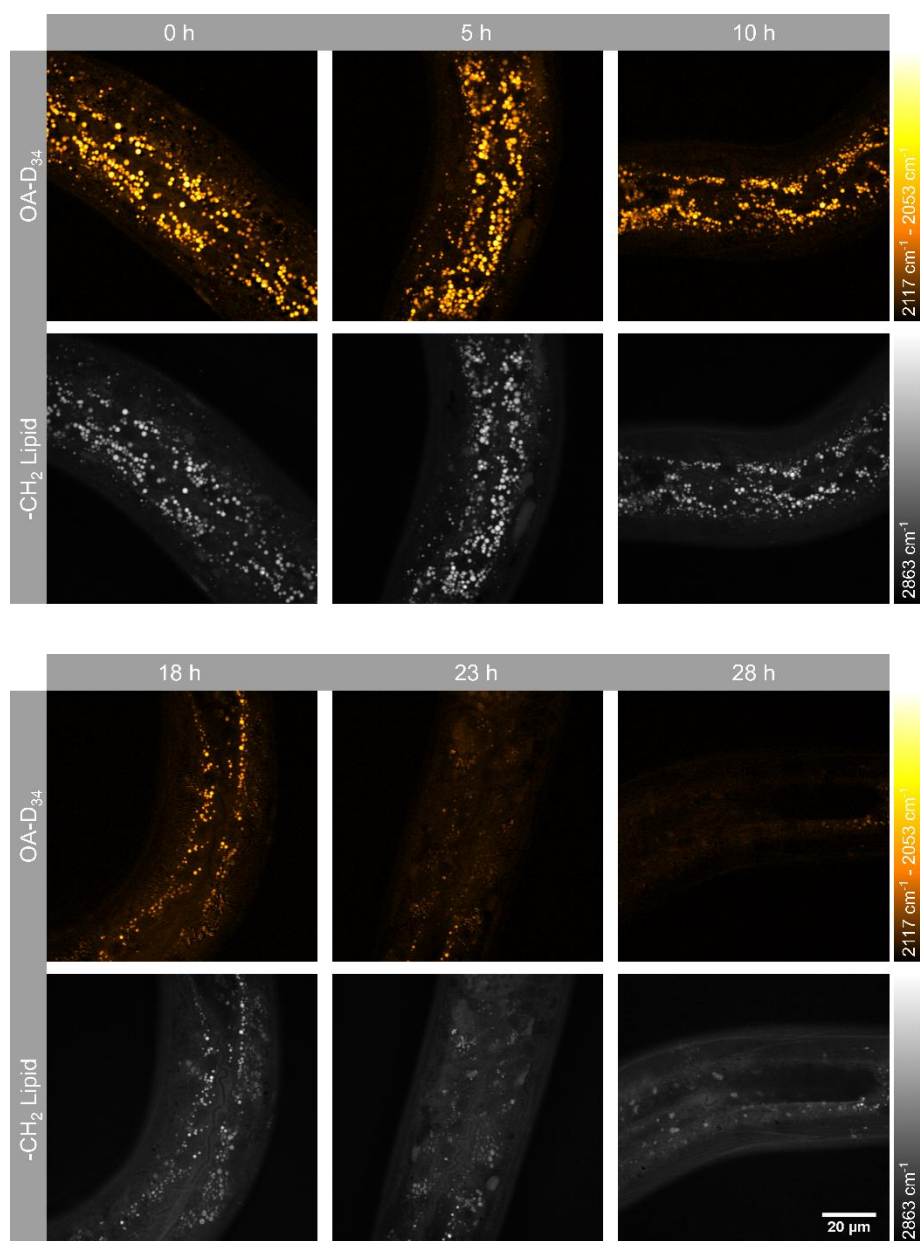**Figure S27.** Representative SRS images of 17-ODYA pre-fed worms during starvation.

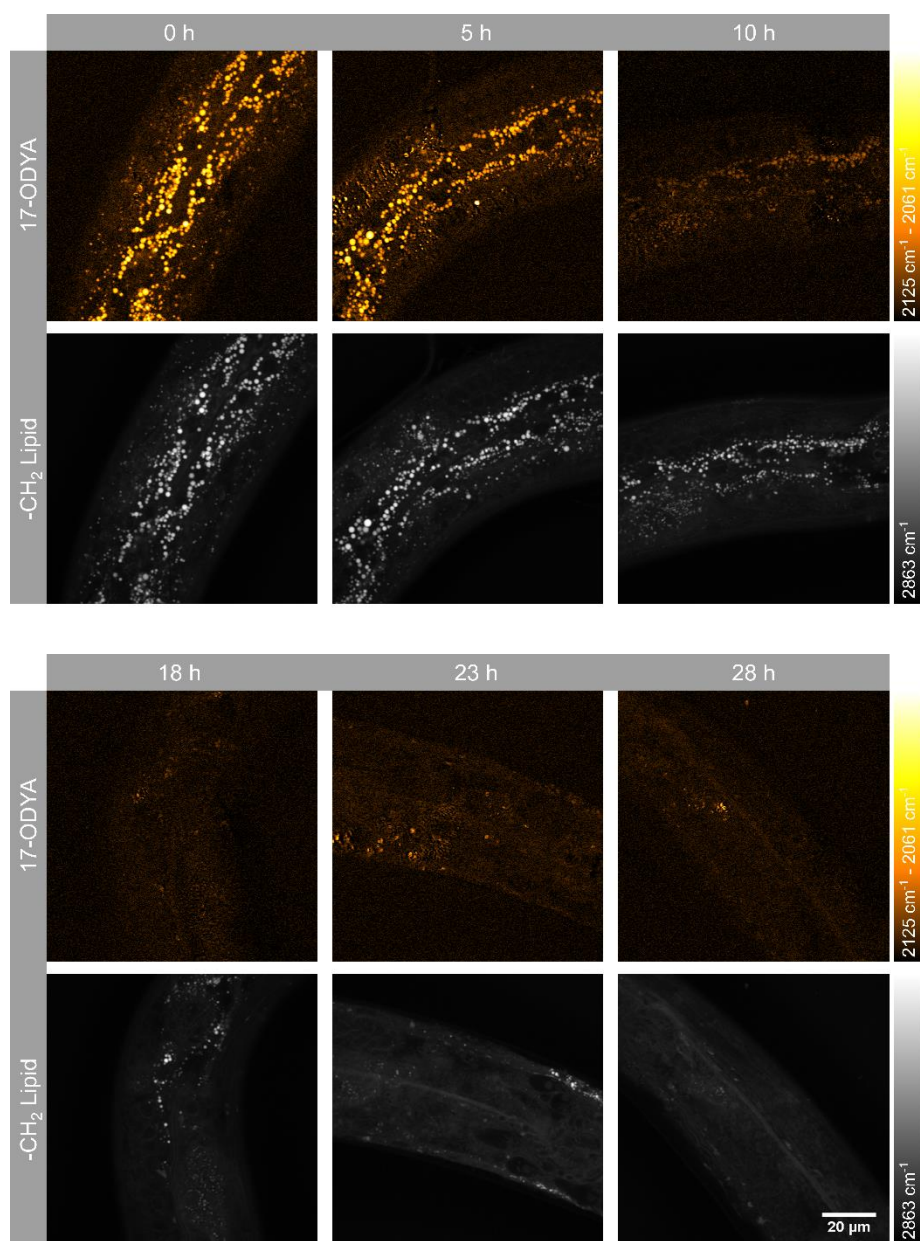**Figure S28.** Quantitative analysis of the size distribution of LDs in anterior region over different starvation times. *: The -CH$_2$ SRS signals at 23 h and 28 h time points were too weak for LDs to be differentiated from surrounding cytoplasm.
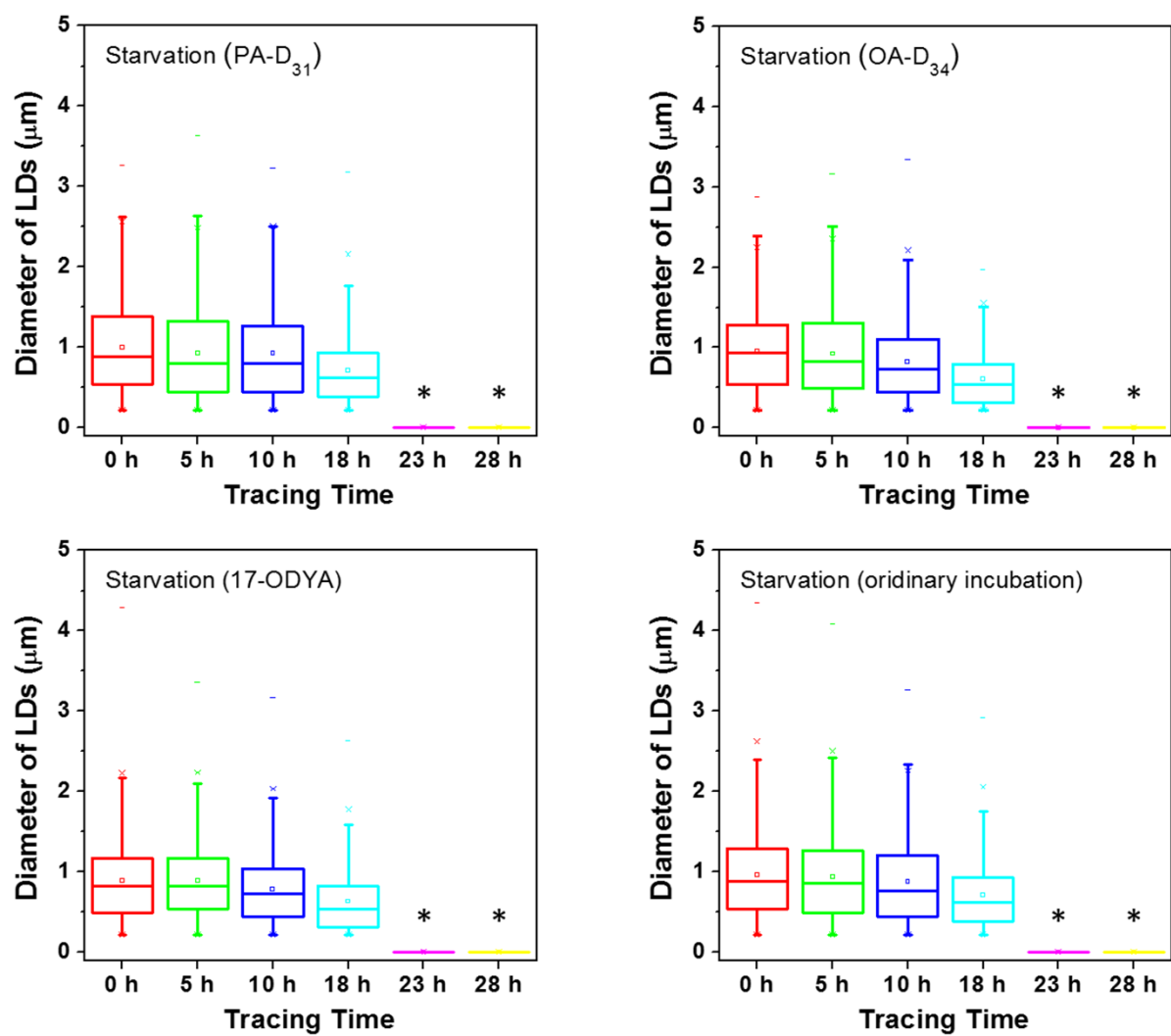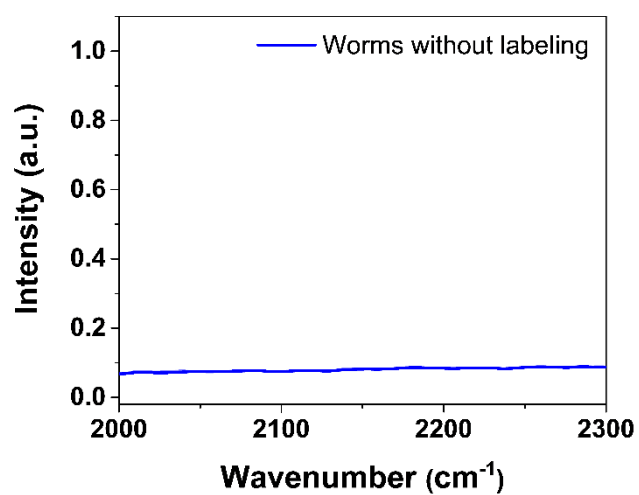
Figure S29. The hsSRS spectra of intestinal LDs in wild-type *C. elegans* without any labeling. See also Movie S5.
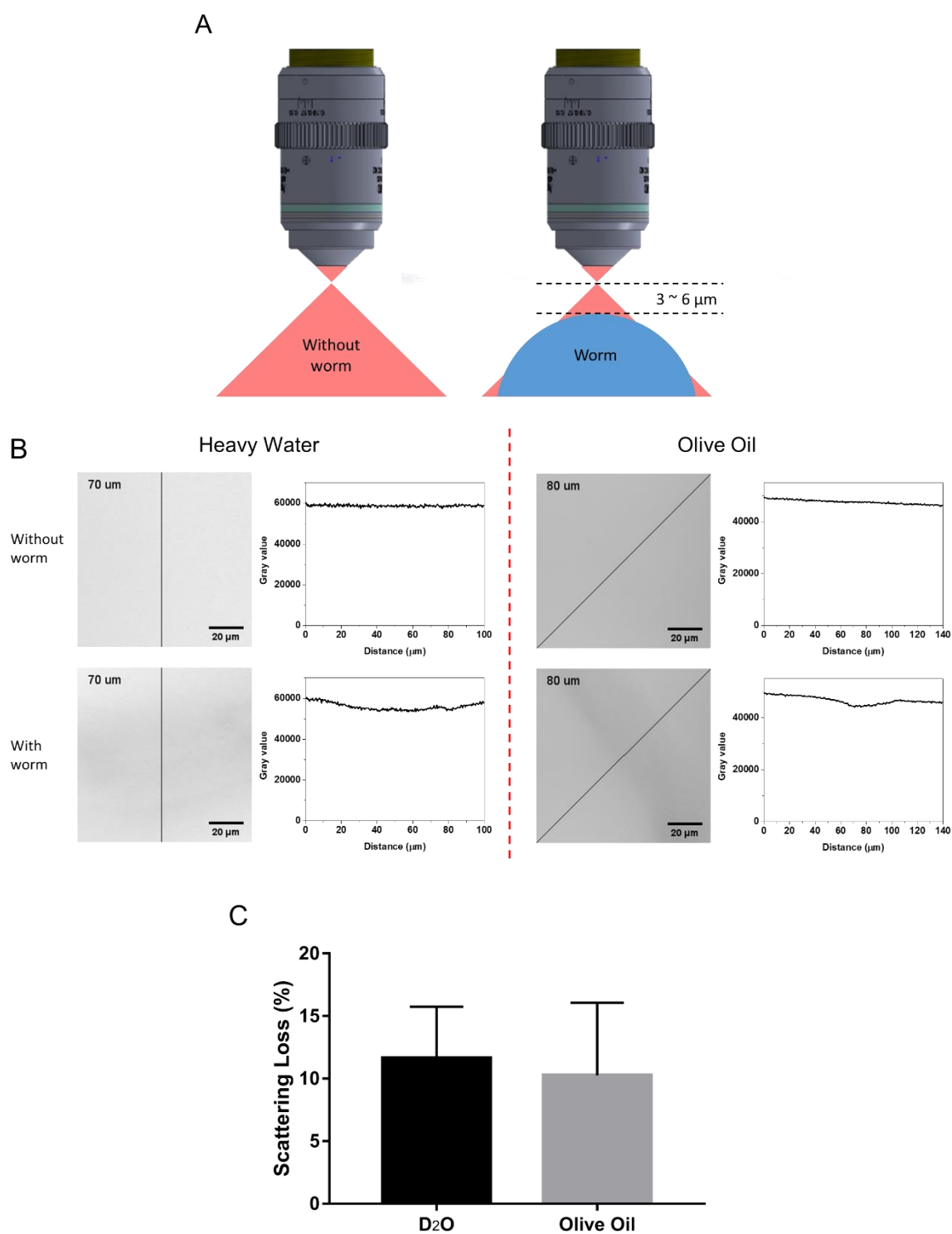
Figure S30. Scattering effects caused by *C. elegans* body on concentration determination. (A) Model of scattering effects in *C. elegans* to SRS imaging. In this experiment, z-scan SRS imaging was conducted in heavy water (820 nm pump beam & 2496 cm⁻¹) and olive oil (796 nm pump beam & 2863 cm⁻¹) with (right) or without (left) worms submerged, respectively. To subject all SRS beams to the potential scattering effect of worm tissues, we took measurements at focal planes 3 ~ 6 μm above the worm (axial resolution of our SRS microscope with 1.15

N.A. objective is 1.3 μm). This depth ensured the whole SRS beam passing through worm body (48 ~ 63 μm in diameter in heavy water and 25~45 μm in diameter in olive oil). (B) Comparison of SRS signals at same depth (3 ~ 6 μm above *C. elegans* body) with and without *C. elegans* below. (C) To quantify the scattering loss, we selected a small area (10 × 10 pixels) in two images recorded at the same depth and calculated the ratio of SRS signals with and without worms below. Statistical analysis demonstrated that the scattering loss caused by *C. elegans* was about 10% (n > 50). In our study of labeled fatty acid quantification, the imaging depth was about 6~8 μm below the worm body surface. The loss caused by worm scattering should not be significantly different from that measured from the region about 3~6 μm above the worm body surface.

The detailed z-scan imaging in heavy water and olive oil samples are shown in Movie S6 and Movie S7.

Movie S1. Z-scanning SRS images of wild-type *C. elegans* at 2863 cm^{-1} CH_2 channel from different depths. (1 μm / step).

Movie S2. Z-scanning SRS images of wild-type *C. elegans* at 2117 cm^{-1} PA-D$_{31}$ channel from different depths. (1 μm / step).

Movie S3. hsSRS images of intestinal LDs in wild-type *C. elegans* labeled with PA-D$_{31}$ for 25 h versus that of PA-D$_{31}$ pure solutions.

Movie S4. hsSRS images of intestinal LDs in wild-type *C. elegans* labeled with OA-D$_{34}$ for 25 h versus that of OA-D$_{34}$ pure solutions.

Movie S5. hsSRS images of intestinal LDs in wild-type *C. elegans* without any labeling (control).

Movie S6. Z-scan SRS imaging of heavy water (2496 cm^{-1}) in which wild-type *C. elegans* have been submerged. (5 μm / step).

Movie S7. Z-scan SRS imaging of olive oil (2863 cm^{-1}) in which wild-type *C. elegans* have been submerged. (5 μm / step).

1. Kong, L.; Ji, M.; Holtom, G. R.; Fu, D.; Freudiger, C. W.; Xie, X. S., Multicolor stimulated Raman scattering microscopy with a rapidly tunable optical parametric oscillator. *Opt. Lett.* **2013,** *38* (2), 145-147.

2. Lu, F.-K.; Basu, S.; Igras, V.; Hoang, M. P.; Ji, M.; Fu, D.; Holtom, G. R.; Neel, V. A.; Freudiger, C. W.; Fisher, D. E., Label-free DNA imaging in vivo with stimulated Raman scattering microscopy. *Proc. Natl. Acad. Sci. U.S.A.* **2015,** *112* (37), 11624-11629.